CEA/SACLAY
DSM

SERVICE DE PHYSIQUE NUCLÉAIRE

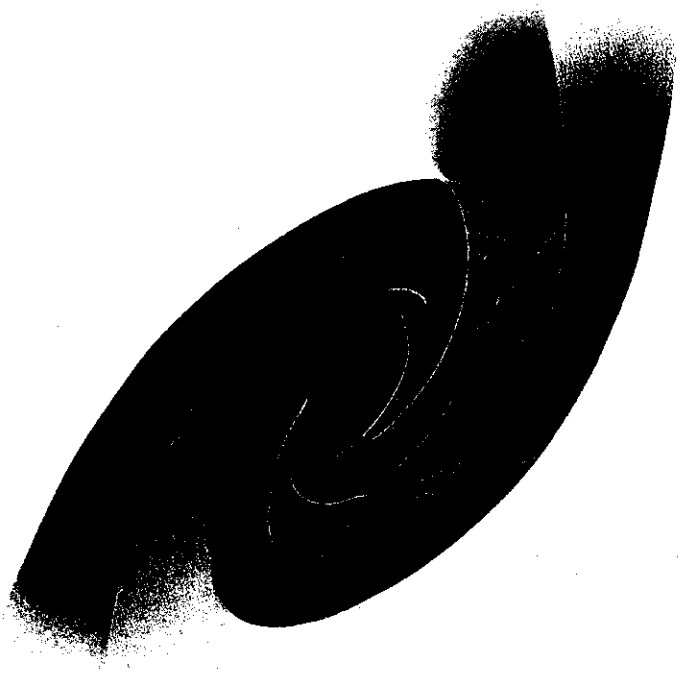

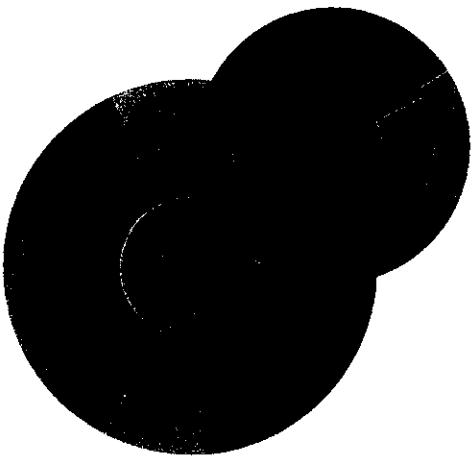

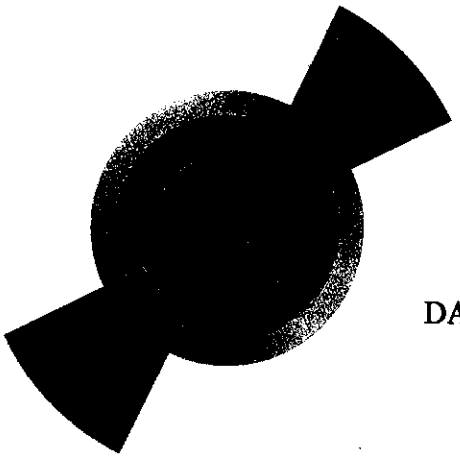

DAPNIA/SPHN-99-12 03/1999

Ternary fission yields of $^{241}Pu(n_{th},f)$

U. Köster, H. Faust, G. Fioni, T. Friedrichs,
V. M. Groβ and S. Oberstedt

DAPNIA

To be published in Nuclear Physics A

Département d'**A**strophysique, de Physique des **P**articules, de Physique **N**ucléaire et de l'**I**nstrumentation **A**ssociée
CEA/Saclay F-91191 Gif-sur-Yvette Cédex

Ternary fission yields of $^{241}Pu(n_{th},f)$

U. Köster [a,1], H. Faust [b], G. Fioni [c], T. Friedrichs [b,d], M. Groß [e] and S. Oberstedt [b]

[a] *Technische Universität München, Physik-Department, 85748 Garching, Bavaria, Germany*

[b] *Institut Laue Langevin, 38042 Grenoble, France*

[c] *CEA Saclay, DSM/DAPNIA/SPHN, 91191 Gif-sur-Yvette, France*

[d] *Technische Universität Braunschweig, Institut für Metallphysik und Nukleare Festkörperphysik, 38106 Braunschweig, Germany*

[e] *Ludwig-Maximilians-Universität, Sektion für Physik, 85748 Garching, Bavaria, Germany*

Abstract

Ternary events in the thermal neutron induced fission of ^{241}Pu(n,f) were studied with the recoil separator LOHENGRIN at the high-flux reactor of the Institut Laue Langevin in Grenoble. Yields and energy distributions could be determined for most isotopes of the elements hydrogen to oxygen. Also several heavier nuclei up to ^{30}Mg could be observed. Yields were measured for 42 isotopes, for further 17 isotopes upper limits could be deduced. For the first time the halo nuclei ^{11}Li, ^{14}Be and ^{19}C were found in neutron induced fission with yields of some 10^{-10} per fission.

Key words: neutron induced fission, ternary fission, ^{241}Pu(n,f), recoil separator
PACS: 25.85.-w, 25.85.Ec, 27.90.+b, 29.30.Aj, 29.30.Ep,

Introduction

More than fifty years ago first experimental evidence for so-called "long range alpha particles" [2] (LRA) stemming from ternary fission was found [1–3]. Since

[1] Corresponding author: Ulli Köster, Email: Ulli.Koster@cern.ch

[2] This notation serves for differentiation against less energetic alphas from radioactive alpha decay.

Article published in Elsevier Preprint NPA (1999) 1–22

then detailed studies of ternary fission[3] were done with different coincidence set-ups, see e. g. [4,5] for an overview. Yields and energy distributions of various ternary particles were measured for several thermal neutron induced fissioning systems: ^{233}U(n,f) [6], ^{235}U(n,f) [7–9], ^{239}Pu(n,f) [10] and ^{241}Am(2n,f) [8–12]. However for other fissioning systems only scarce data existed, which made a systematic study of the dependence of yields and energy distributions of ternary particles on the fissility and neutron excess of the compound system difficult.

There is still no theory which could reproduce the individual yields and energy distributions of ternary fission fragments from first principles. Only in the special case of alpha accompanied fission of ^{236}U* a numerical solution of the Schrödinger equation describing "alpha decay during fission" was possible and gave roughly correct values for the absolute emission probability and energy distribution of the alpha particles [13]. A similar approach had been used by Cârjan to reproduce average energy and emission probability of LRA in ^{236}U* [14,15]. For cold spontaneous ^{10}Be accompanied fission of ^{252}Cf the relative probabilities of the associated fragment mass splits have been calculated recently [16], but the inverse problem, i.e. the calculation of individual ternary particle yields with a fixed or averaged mass split for the light and heavy fragments, has not been attacked yet. The random neck rupture model of Rubchenya and Yavshits [18] can explain the LRA emission probability in different fission systems, but to reproduce the yields of individual ternary particles a fit to experimental data is used. Several other semi-empiric ternary fission models exist [17,19–22], but they also require a basic set of yield data to fit the free constants.

Very low yields of fission products can be measured with a recoil separator. To date the most sensitive recoil separator is LOHENGRIN at the high-flux reactor of the Institut Laue Langevin (ILL) in Grenoble. Recently a series of measurements was performed at LOHENGRIN to study the ternary fission of: ^{229}Th(n,f) [23], ^{233}U(n,f) [24,25], ^{239}Pu(n,f) [23,25], ^{241}Am(2n,f) [26], ^{245}Cm(n,f) [25,26] and ^{249}Cf(n,f) [27].

Here we will report on the investigation of ^{241}Pu(n_{th},f), where before only data for the two most abundant and technologically important ternary particles existed. The yield of ^{4}He had been determined to $(1.86 \pm 0.05) \cdot 10^{-3}$ per binary fission and the yield of ^{3}H to $(1.41 \pm 0.06) \cdot 10^{-4}$ per binary fission or (7.61 ± 0.19) % of the ^{4}He yield [28].

[3] In fact, here we are not discussing "true" ternary fission with a breakup in three fragments of about equal size, but a process where additionally to two heavy nuclei with masses comparable to binary fragments a light charged particle is emitted. For brevity we will call this process of "light charged particle accompanied fission" just ternary fission or tripartition.

Experiments

Targets

In total four different targets were used. They were prepared by the IRMM (Institute for Reference Materials and Measurements) of the Joint Research Centre of the European Commission in Geel. The plutonium oxide was deposited within an area of $70 \cdot 5$ mm^2 on a platinum-coated [4] titanium backing. A "thin" target with 208 μg Pu per cm^2 thickness was used to determine during a measurement of binary fission [29] the yield of ^{10}Be as a reference point for further ternary fission measurements. Another "thin" target (100 μg/cm^2 Pu) was used to measure exactly the energy distribution of the helium isotopes down to 3 MeV. Two "thick" targets with 379 and 362 μg Pu per cm^2 thickness served for the measurement of ternary fission yields relative to ^{10}Be. The first three targets had in November 1990 an isotopic composition of 87 % ^{241}Pu, 1.6 % ^{239}Pu and 11 % other plutonium isotopes with low fission cross sections. At the time of the measurements about 20 %, 31 % and 28 % respectively of the ^{241}Pu had decayed to ^{241}Am, but as discussed in [30] during two weeks of measurement [5] the contribution of other fission systems (e.g. from breeded ^{242}Am(n,f)) will stay below 6 %. The last target was used 9 months after plutonium separation, thus limiting contributions from other fission systems to below 2 %. The targets were covered with a 2500 Å thick nickel foil to reduce loss of target material by sputtering and thus guarantee a smoother burnup.

Separator

The targets are brought in an evacuated beam tube of the ILL high-flux reactor (58 MW thermal power and $1.5 \cdot 10^{15}$ cm^2 s^{-1} maximal unperturbed thermal flux). At the target position, about 50 cm from the reactor core, the thermal neutron flux is about $5.3 \cdot 10^{14}$ cm^2 s^{-1}. The epithermal neutron flux is more than two orders of magnitude smaller and the fast neutron flux is more than three orders of magnitude smaller. Both contributions can be neglected for our purposes. Recoiling fission products leave the target with a small energy loss and fly as highly charged ions through the beam tube. While binary fragments have typically ionic charges of 20 to 25, light ternary particles are mostly fully stripped. After 8 m the ions enter a horizontally deflecting homogeneous magnetic sector field, separating ions according to the ratio of momentum

[4] The 400 μg per cm^2 thick Pt layer reduces the diffusion of plutonium into the Ti backing.

[5] The second target was kept not even 48 h in the neutron flux.

to ionic charge p/q. Subsequently they pass a vertically deflecting cylindric condenser, which provides a separation according to the ratio of kinetic energy to ionic charge E/q. Both fields are arranged to the double focusing parabola spectrometer LOHENGRIN [31,32], separating ions of the same A/q ratio onto a parabola, on which the position is given by the kinetic energy of the ion [33]. For cases where no ultimate energy resolution is needed, but rather a high beam intensity or transmission should be achieved, a second magnet was designed which focusses about 40 cm of the mass parabola to a small area (some cm^2), see figure 1. This so-called RED (Reverse Energy Dispersion) magnet [34] was used for the measurements with the "thick" targets, while the measurements with the "thin" targets were made without RED magnet.

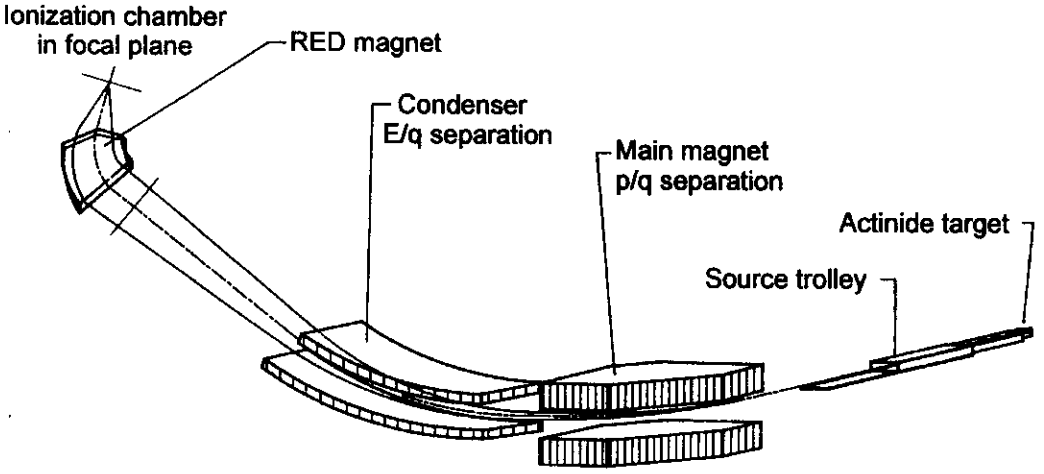

Fig. 1. Arrangement of the recoil separator LOHENGRIN.

Whereas the usable range of magnetic fields (up to 0.24 T for the first magnet and maximal 1.6 T for the RED magnet) is sufficient to cover most of the required separator settings, the maximal high voltage of the condenser limits the E/q ratio to about 6.5 MeV, thus excluding the measurement of high kinetic energies at low charge states.

The flight time of the fragments from the target to the detector is below 2 μs. Thus decay losses of the studied particles with halflives larger than milliseconds can be neglected.

Particle identification

LOHENGRIN only separates particles according to their A/q and E/q ratios. For an unambiguous determination of the fragment mass it is still necessary to measure directly the kinetic energy of the fragments. With the known settings for E/q and A/q thus the ionic charge q and finally the mass A can be determined. The kinetic energy is measured with an ionization chamber

placed in the focus of the separator. Using a split anode for the readout of the energy signal, additionally the nuclear charge Z can be deduced from the specific energy loss in the first section of the ionization chamber, the so-called ΔE part. The used ionization chambers are described in detail in references [35,36]. The counting gas (isobutane) pressure was adapted in the range of 15 to 160 mbar for best Z identification. In all cases the Z-resolution of the ionization chamber was by far sufficient for a clear identification of the ternary particles.

Calibrations

Magnet calibration

During the measurement the magnetic fields are controlled with NMR probes and stabilized to some 10^{-5}. However the NMR probe measures the field only locally, whereas the particles are deflected according to the integrated field along their flight path. Hysteresis and remanence effects may change the calibration of the magnet. The optimum magnetic field settings are found by scanning the beam horizontally over the detector placed in the focus, while keeping the electrical field fixed. The so determined magnet constants, called χ (for the first magnet) in [37] and κ (the ratio of fields of RED to first magnet), stayed constant within a range of $\leq 2 \cdot 10^{-4}$ during the measurement periods of about 2 weeks.

Energy calibration

The absolute energy calibration of the separator can be checked with direct (n,X)-reactions producing monoenergetic particles. The electric and magnetic fields are scanned simultaneously to find the high energy edge of the energy distribution, which has typically a low energy tail due to energy loss in the target and scattered particles, see figure 2.

Three reactions were used:

(1) ^{6}Li(n,α)t giving tritons with 2.73 MeV kinetic energy and alphas with 2.05 MeV. These calibrations are done "off-line" by introducing a thin ^{6}Li target at the target position [37].
(2) ^{59}Ni(n,α) giving alphas with 4.78 MeV kinetic energy. The unstable ^{59}Ni is produced "on-line" by neutron capture on ^{58}Ni present in the nickel foil which is used to cover the target.
(3) Decay alphas of ^{242}Cm with up to 6.11 MeV. The ^{242}Cm is here produced by beta-decay of ^{241}Pu to ^{241}Am which is subsequently transmuted to ^{242}Am by neutron capture and then decays to ^{242}Cm. Also this reaction

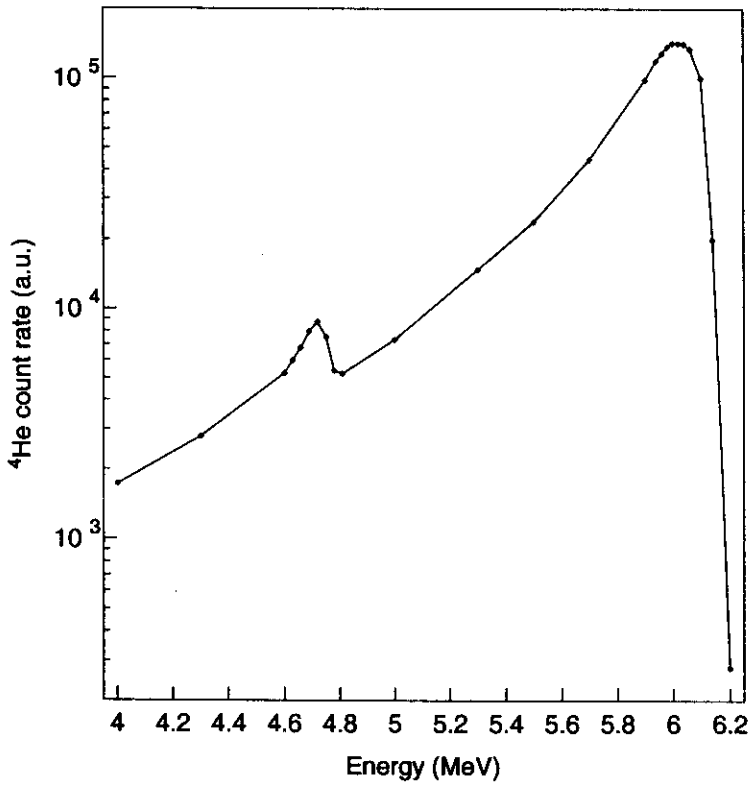

Fig. 2. Energy spectrum of ^{4}He used for on-line energy calibration. The peak around 6.1 MeV is due to decay alphas from ^{242}Cm and the peak at 4.78 MeV comes from ^{59}Ni(n,α). Shown is a raw spectrum without correction for energy loss in the target and cover foil.

is used "on-line" without target change.

Calibration of the ionization chamber

The energy and nuclear charge calibration of the ionization chamber was done with reference spectra using separator settings $A/q = 3$. Here the most abundant ternary particles (^{3}H, ^{6}He, etc.) and scattered stable isotopes (e.g. ^{12}C, ^{24}Mg, ^{27}Al) are easy to identify and make the calibration obvious, see figure 3.

Data evaluation

Background

Instabilities of the high tension or sparks in the condenser can cause background in the ΔE/E scatter plots. Scattered binary particles occur especially with separator settings close to typical values for binary particles ($A/q = 4$ to

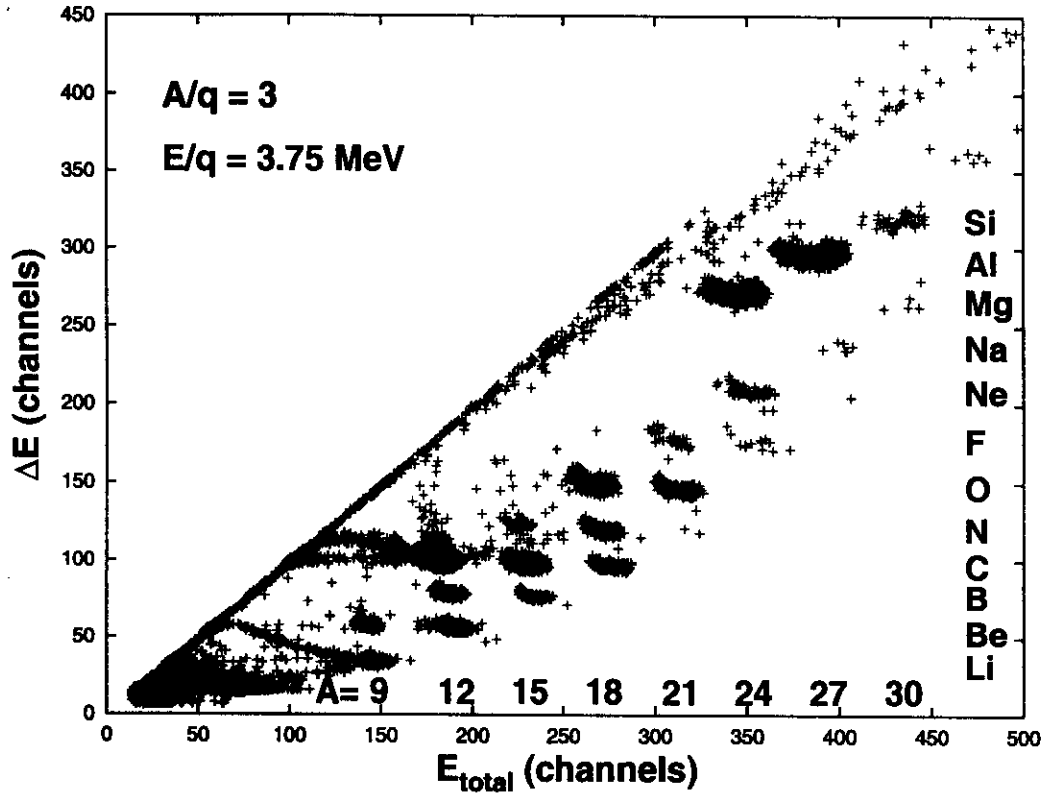

Fig. 3. ΔE-E-scatter plot with separator setting $A/q = 3$ and $E/q = 3.75$ MeV. The measurement time for this spectrum was 6.1 h. The horizontal scale is proportional to the particle energy (and due to a fixed A/E ratio also to the mass), whereas the vertical scale is roughly proportional to the nuclear charge Z. Scattered binary particles create background close to the diagonal in the upper part of the spectrum. Background in the lower part is due to pile-up (from abundant ^{3}H and ^{6}He) and particles scattered in the entrance window of the ionization chamber (tails going to the top and left which can be seen at ^{6}He, ^{9}Li and ^{12}C). One channel corresponds approximately to 75 keV.

5, E/A around 1 MeV).

High background from natural alpha decay and (n,α) reactions is present for ^{4}He below 6.1 MeV. Also for ^{3}H below 2.7 MeV significant background arises from ^{6}Li(n,α) reactions. This ^{6}Li is sputtered off from calibration targets (see above) and sticks to the target holder or the beam tube. For these cases only the data points with higher kinetic energy are evaluated.

Some stable particles (^{12}C, ^{14}N, ^{16}O, etc.) occur very abundantly. They are knocked out by fission fragments from the target and its cover, from the residual gas in the vacuum chamber or from diaphragms in the separator. Their abundance drops rapidly down towards higher kinetic energies. However, if the contribution of such background gets too high, the events stemming from fission cannot be identified and no fission yield can be determined for these stable isotopes.

Typically the background conditions are more favorable for isotopes with a large neutron excess than for proton-rich isotopes. This explains partly the great differences in measured upper limits for rare ternary isotopes on the neutron-rich and the neutron-deficient side.

Separator acceptance

The energy dispersion coefficient[6] of the separator is 7.2 m, i.e. a 1 % large slice of the energy distribution is spread out over 7.2 cm of the mass parabola. The accepted energy range is therefore proportional to the chosen energy. To correct this effect, all count rates are divided by the set energy for normalization.

In mass direction (i.e. perpendicular to the mass parabola) the dispersion coefficient[7] is 3.24 m. Due to the different mass defects, the difference between ionic mass and atomic mass depending on the charge state and relativistic corrections not all isotopes with the same A/q ratio lie exactly on the mass parabola. The actual transmission is a complicated function, which could be calculated by folding the size of the target with the transmission through intermediate diaphragms and vacuum chambers, the edge focussing by the RED magnet and the acceptance of the circular entrance window of the ionization chamber. It can also be experimentally deduced from the scan curve of the main magnetic field (see figure 4). The FWHM is typically 0.2 to 0.3 % of the magnetic field. For small deviations from the ideal field the yield of a given isotope is corrected for the transmission, in case of larger deviations (e.g. for the light particles ^{3}H, ^{6}He, etc. in a spectrum with $A/q = 3$) two spectra with different magnetic field settings have to be taken. The scan curve of the RED magnet is much broader (FWHM some %), therefore no correction is necessary.

Target burnup

The fission rate of the target decreases with time. This is mainly due to the nuclear burnup in the high neutron flux. Additional losses of target material occur from sputtering by fission fragments, evaporation from the heated target and diffusion into the target backing. The slight reduction of the neutron flux (about 3 % during one reactor cycle of 52 days) can be neglected. The decrease

[6] Particles with a kinetic energy $E_0 + \Delta E$ are separated in the plane of dispersion by a distance Δx from the reference particles with energy E_0. For small deviations ($\Delta E \ll E_0$) the linear relation with the energy dispersion coefficient D_E applies: $\Delta x = D_E \frac{\Delta E}{E_0}$.

[7] In analogy to the energy dispersion the mass dispersion coefficient D_m is defined as: $\Delta x = D_m \frac{\Delta m}{m}$.

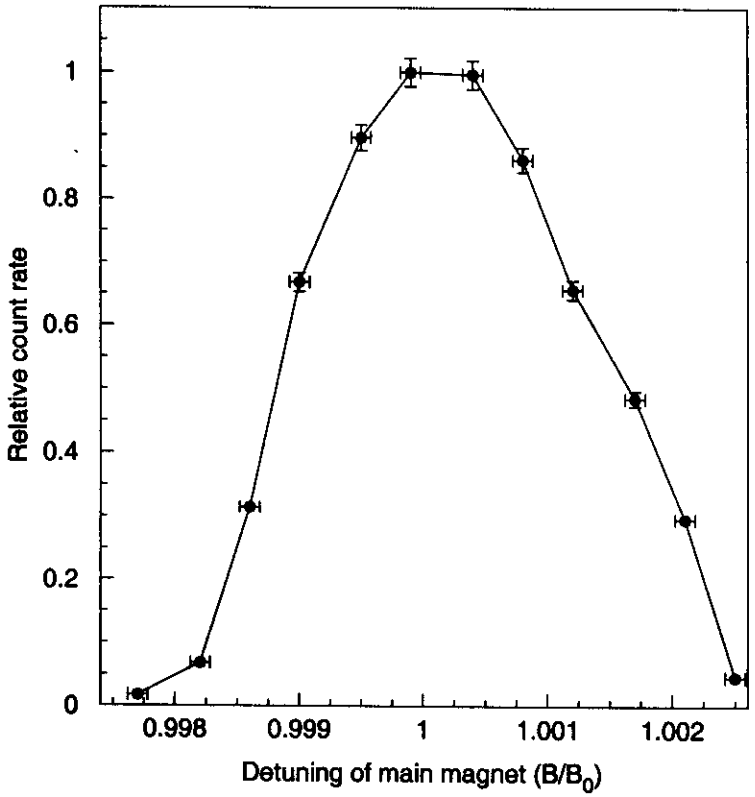

Fig. 4. Measured transmission in dependance of a detuning of the main magnetic field.

of the fission rate is monitored with a reference spectrum taken once to twice a day and can be described with an exponential decay curve.

It should be noted that plutonium targets can show a less regular burnup characteristic than other actinide targets. This might be due to a rapid migration into the target backing or sidewards out of the target area (see also [30]). The former explanation is supported by differing burnup times for heavier and lighter isotopes and a broadening of the "natural" width of the energy distribution. These effects are difficult to quantify, but contribute to the systematic errors. For very precise measurements plutonium targets cannot be used "completely", but should be changed after some days.

Energy loss

To deduce the original kinetic energy distribution of the fission fragments from the measured one, the energy loss in the target and in the cover foil has to be taken into account. The energy loss for all measured isotopes and kinetic energies was calculated with the Monte-Carlo program TRIM [8] [38]. Note that

[8] Since TRIM does not contain transuranium elements as target, the calculation was performed for uraniumoxide and scaled. The resulting uncertainty is negligible.

the energy loss in the entrance window of the ionization chamber occurs after the mass separation and has therefore not to be considered here.

Ionic charge distribution

Due to the limitations of the separator fields and the available beam time it is not possible to measure the yields of a given isotope at all possible ionic charge states. Therefore a model has to be applied to inter- and extrapolate the ionic charge state fractions to other energies and isotopes. Several empiric formulae are available to predict the mean ionic charge states, the width of the charge state distribution and thus allow to calculate the equilibrium charge state distributions (ECSDs) [39–47]. However, the ECSDs used for these formulae were measured under well defined experimental conditions, mostly by transmitting low charged ions from tandem accelerators through free-standing foils made from pure materials. On the other hand at LOHENGRIN the charge state before passing the foil is not well known. Moreover the target cover foils are quite fragile (0.25 μm of nickel) and coated with a protective film of acrylic or polystyrene for better handling. The nuclear heating in the reactor will bring the target to above 600° C and the coating evaporates. Still some atomic layers of e.g. carbon may be left and then influence the ECSDs. Therefore the constants of such formulae have to be determined for each target by measuring in-situ the ECSDs of appropriate isotopes (^{10}Be, ^{14}C, ^{20}O).

None of the investigated formulae was able to reproduce the ECSDs of all elements with a given set of constants or with one single fit parameter. For better comparison with other LOHENGRIN measurements we finally used a modified reduced chi-square distribution with a parametrisation in analogy to the data evaluation of [9,12,24,26].

The mean charge is calculated as:

$$\bar{q} = \left(Z + \frac{1}{Z^2}\right) \cdot \left(1 - \exp\left(-2.7284 \cdot v_{ion} \cdot \left(Z + \frac{1}{Z^2}\right)^{\frac{0.5}{\lambda} - 0.48}\right)\right) \quad (1)$$

and the width of the charge state distribution is:

$$\sigma_q = \left(0.426 - \mu \cdot v_{ion} \cdot \left(Z + \frac{1}{Z}\right)^{-0.475}\right) \cdot \left(Z + \frac{1}{Z}\right)^{0.447 - \frac{1}{\lambda^2}} \quad (2)$$

with two fit parameters λ and μ depending on the element and target. v_{ion} is given in units of cm/ns. This expression for $\bar{q}$ is, with exeption of the small modifications by λ and $1/Z$, identical to that of [43]. σ_q is similar to formula (6) in [44].

The fraction of an individual charge state can be calculated with a "reduced chi-square distribution" [44], modified by a factor $\exp(-a)$.

$$F(q) = \frac{c \cdot t(q)^{\frac{n}{2}-1}}{2^{\frac{n}{2}} \cdot \Gamma(\frac{n}{2}) \cdot \exp(\frac{t(q)}{2})} \cdot \exp(-a) \tag{3}$$

with Γ being the gamma function and the constants:

$$\begin{aligned} c &= \frac{2 \cdot (Z - \bar{q} + 2)}{\sigma_q^2}, \\ t(q) &= c \cdot (Z - q + 2), \\ n &= c \cdot (Z - \bar{q} + 2), \\ a &= \left(\frac{v_{Z-q+1}}{v}\right)^{\sqrt{1+\frac{Z}{\lambda}}} \end{aligned}$$

where $\exp(-a)$ gives the stripping probability for the $(Z\text{-}q{+}1)$th electron. Its orbital velocity in the Bohr model v_{Z-q+1} is calculated from the qth ionization energy given in [49].

The parameters λ and μ had to be adapted for each element. It appeared, that λ differed strongly between the third and fourth target [9]. This could be explained by different evaporation residues on the target cover foil. In the former case the nickel foil was covered by an acetate film, in the latter by a polystyrene film. On the other hand μ showed only a weak variation (ranging from 0.02 to maximal 0.025). It is possible to fit the constants by using the measured charge state fractions of different isotopes of one element up to about oxygen. Figure 5 shows one of the fitted ECSDs for ^{14}C. For these light elements the ECSDs formula is mainly used for interpolation of the measured charge state fractions and simplifies a transfer of these ratios to other isotopes of the same element. The systematic errors are therefore acceptable. However, for lack of experimental data [10], the trends of the charge state distribution have to be extrapolated towards heavier elements. Here it had to be assumed as in [26], that, compared to the big differences for light elements, the variation

[9] With the second target only helium isotopes were measured. The contributing charge states (2+ and below 2.5 MeV per nucleon also 1+) can be measured directly and no elaborate ionic charge correction is required.

[10] It is in principle possible to measure also the ECSDs of elements like Mg, Si, etc. in a dedicated experiment at LOHENGRIN. Instead of ternary particles, stable isotopes of these elements would be used which are knocked out from an additional layer containing the elements in question between the actinide and the cover foil by collisions with binary fragments. In this way the constants could be pinned down much better even for heavier elements, reducing the systematic errors significantly.

of the fitting constants from element to element continue to decrease and the "constants" can be kept constant. The uncertainty of this extrapolation creates the dominating part of the systematic errors.

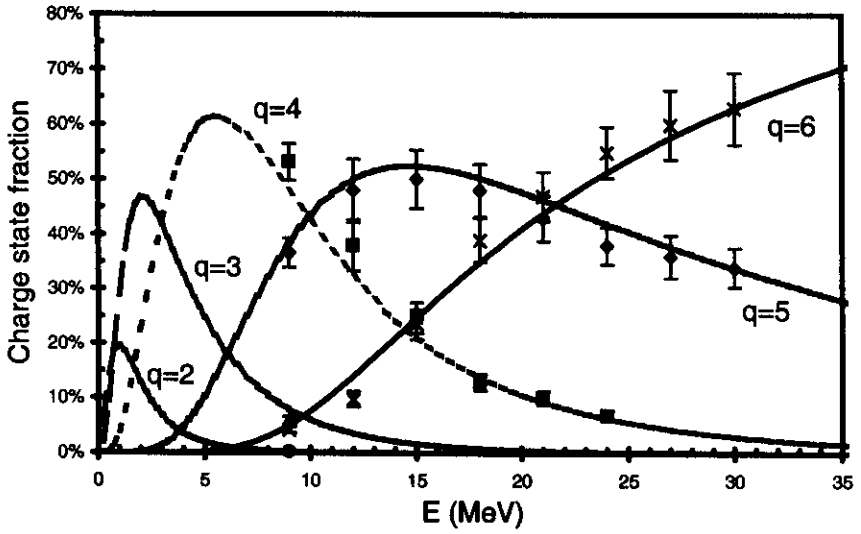

Fig. 5. Measured charge state fractions and fitted charge state distribution for ^{14}C.

Kinetic energy distribution

The total yield of an isotope is determined by integration over its yield at different kinetic energies. In cases where, due to limitations in electric field or beam time, not enough different energies could be measured to determine the energy distribution, the mean energy and/or the width of the energy distribution had to be fixed for the fitting. For ^{4}He we used the mean energy and width from [28]. For ^{3}H we also used the mean energy from [28], but kept the width as a free fit parameter. For ^{2}H we employed also the mean energy of ^{3}H, which is justifiable regarding the systematics of other fission systems [4]. For the rare isotopes we used an extrapolation which is consistent with the systematics in other fission systems and the results of trajectory calculations for the nearby fission system ^{242}Am(n,f) [9,21]. In all cases where the energy parameters were fixed for the fit, an additional systematic error was added to account for the uncertainties of these values.

Practically all energy distributions are well reproduced by a Gaussian. An exeption is ^{4}He. It is well known [50], that the low energy part of the ^{4}He spectrum shows an enhancement over a symmetric Gaussian distribution, probably due to contributions from the breakup residues of the particle unstable isotopes ^{5}He and ^{8}Be [5]. Therefore we used only the data points with energies above 10 MeV for the integration of the yield.

Results

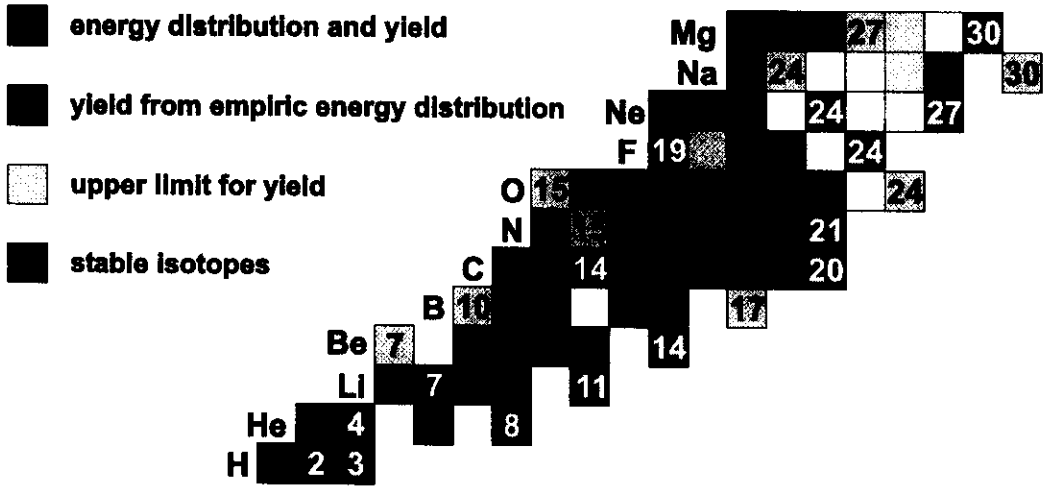

Fig. 6. Overview of the measured ternary particles arranged in form of a nuclide chart. The numbers mark the mass of the lightest and heaviest measured isotope of each element.

Figure 6 shows an overview of the measured isotopes. The detailed data are given in tables 1 and 2. E_{mean} and E_{FWHM} are obtained by fitting a Gaussian distribution to the data points. Cases where these values were taken from systematics are marked by the label "*fix*" in the row of the corresponding uncertainty. For better comparison to other fission systems the yields are normalized to a standard of 10000 for ^{4}He. Note that the reference point itself has a rather large error since the yield of ^{4}He can only be determined from a small energy range (10 to 13 MeV) [11]. An additional systematic error (difficult to estimate and not included in table 1) could occur if the energy distribution showed a non-Gaussian behaviour in the fit range. The given errors are the individual errors for each isotope and do not include the error of the reference point.

In LOHENGRIN measurements the light charged particle is detected without coincidence to the heavy fragments. Its origin from ternary fission [12] has therefore to be deduced from its kinetic energy distribution. Tables 1 and 2 show the maximal kinetic energy E_{bin} which the light charged particle could attain in case it is produced in a binary reaction, e.g. ^{241}Pu(n,α)^{238}U. A dash indicates that the Q-value of such a direct reaction is negative, i.e. the reaction is impossible with thermal neutrons. No entry is made in cases where the

[11] The upper limit is given by the maximally achieved voltage in the LOHENGRIN condenser.

[12] It could also come from quaternary fission, however such an event was never observed and should be much rarer than ternary fission. Breakup fragments from decay of excited ternary ^{7}Li* and of ^{8}Be which can give experimentally the impression of quaternary fission are discussed in [52,53].

mass of the potential heavy binary partner is unknown [51]. Especially for the lighter isotopes it is evident from the high measured energies that they are indeed produced in ternary fission.

Figure 7 shows a plot of the individual isotopic yields. The strong proton even-odd effect which favors emission of ternary particles with even Z is obvious (see also figure 9). Also the less pronounced neutron even-odd effect is clearly visible (staggering within one element).

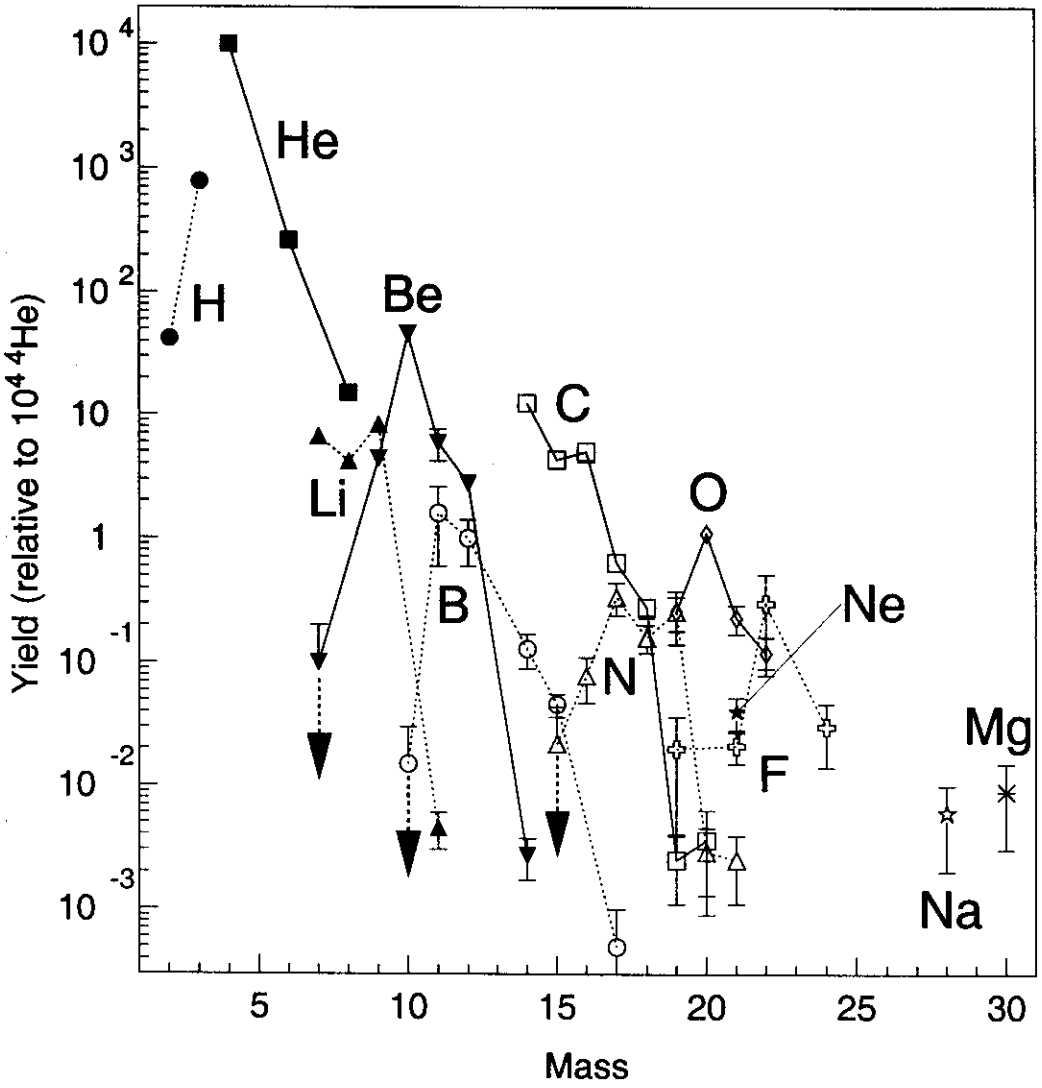

Fig. 7. Measured yields of ternary particles normalized to 10^4 for ^{4}He. The isotopes of each element are connected by a line, dashed for odd Z and solid for even Z. Upper limits are marked with an arrow. Some upper limits have been omitted for sake of clarity.

The integrated mass and elemental yields are shown in figures 8 and 9 respectively. For complete summing the missing individual yields (e.g. for mass 13 nuclei) were interpolated from neighbouring yields according to the ratios pre-

dicted by the Faust formula [22]. Contributions from particle unstable nuclei are neglected. The mass yields were converted to absolute yields (per fission) with the ternary to binary ratio from [28]. For comparison the binary yields of the light fragment group from [30,54] are also plotted. The strong oscillation (see figure 8) of the ternary yields can be understood from the fact that most ternary mass yields are dominated by a single isotope. Thus high yields of individual isotopes (e.g. ^{10}Be, ^{14}C, ...) lead to a significant staggering of the yields.

The detection limit for ternary particles is around 10^{-10}. Figure 10 shows that isotopes with large neutron excess can, despite their extremely low yield, be clearly and unambiguously identified in the ΔE-E-scatter plot. Thus also the neutron halo nuclides ^{11}Li, ^{14}Be and ^{19}C could be identified with absolute yields of $8.4(28)\cdot10^{-10}$, $5.0(19)\cdot10^{-10}$ and $4.7(26)\cdot10^{-10}$ per fission respectively.

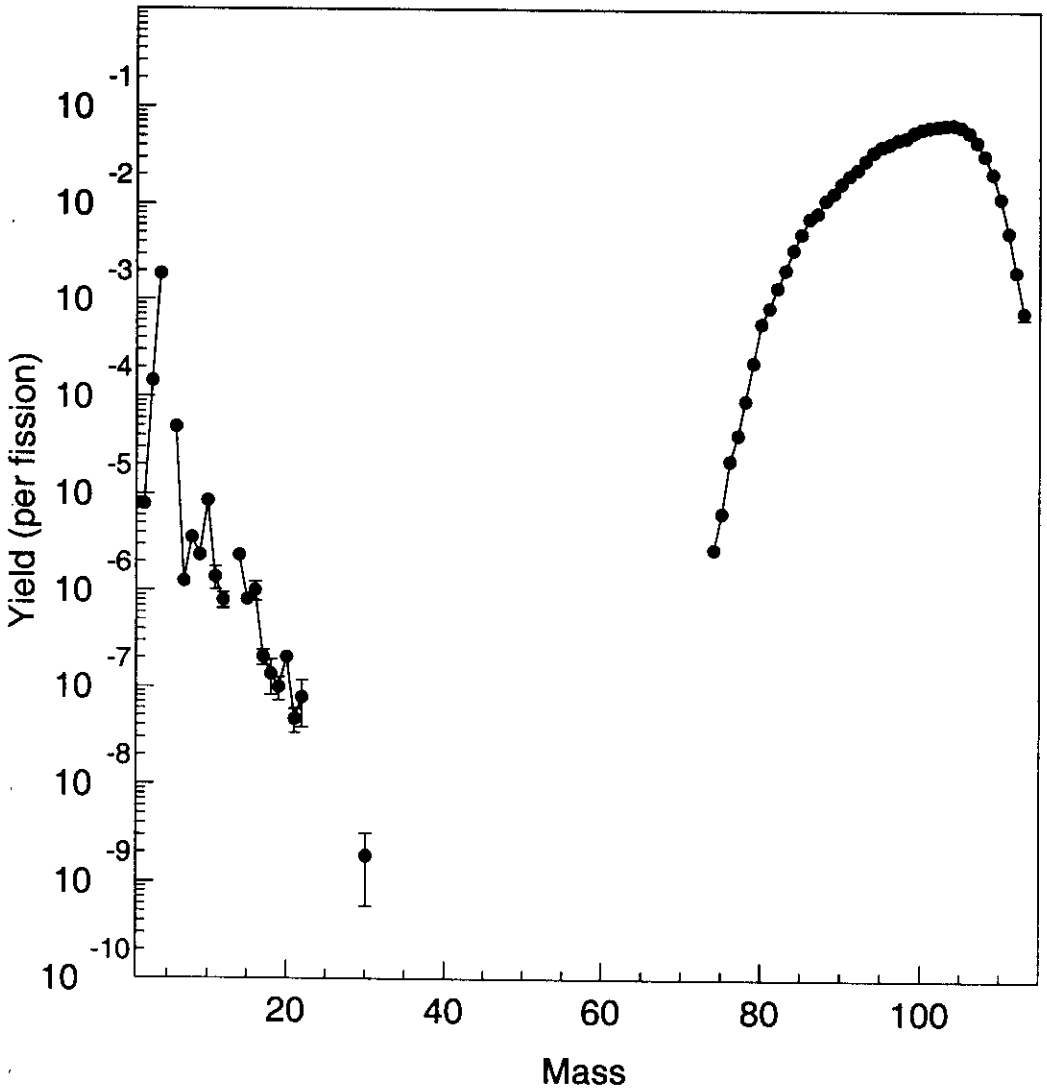

Fig. 8. Absolute mass yields from ^{241}Pu(n_{th},f) in events per fission.

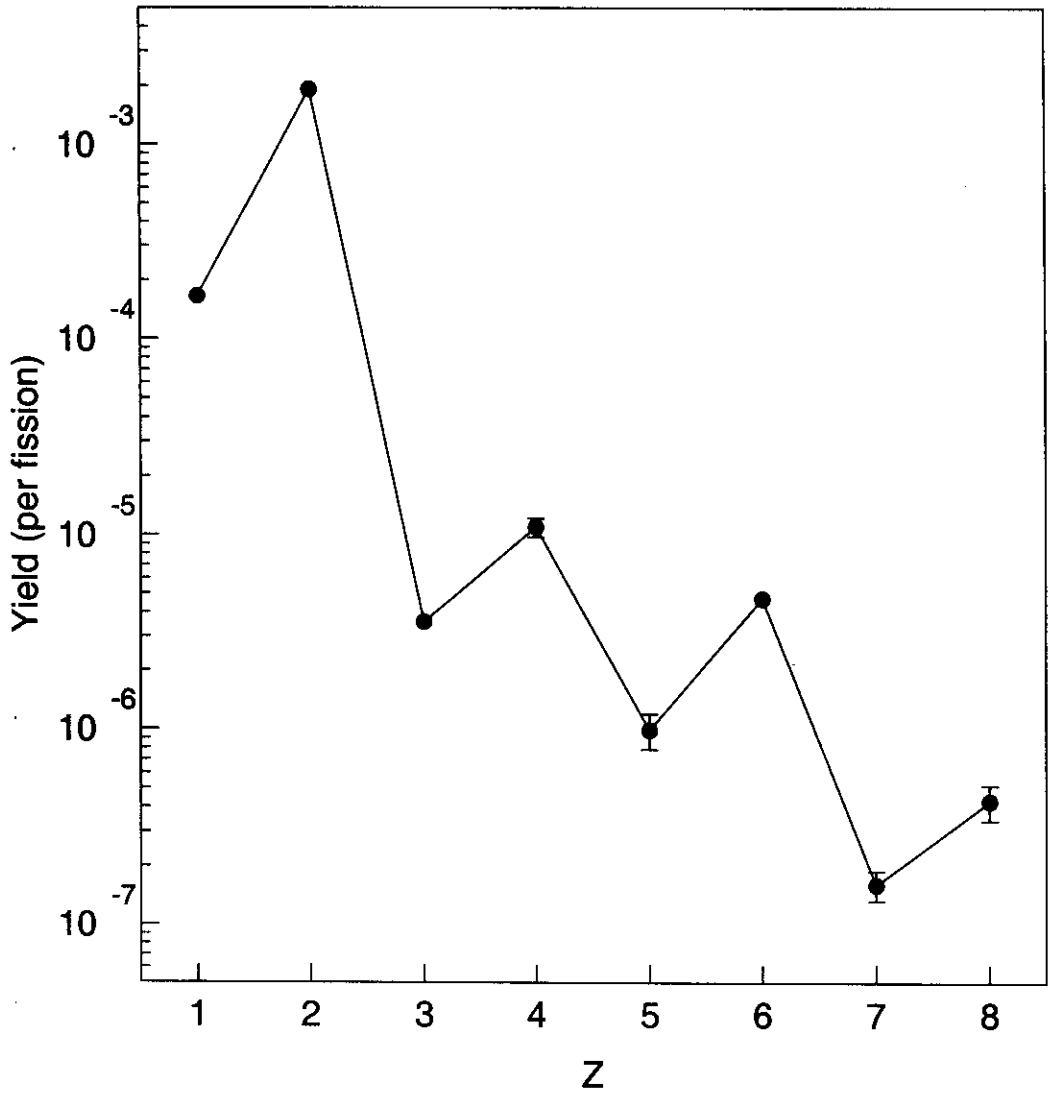

Fig. 9. Elemental yields of ternary particles in events per fission. A possible contribution of low-energy (polar) protons to the hydrogen yield was neglegted.

Summary and Outlook

Ternary fission of ^{241}Pu(n_{th},f) was studied and yields and energy distributions could be determined for most isotopes of the elements hydrogen to oxygen. Also several heavier nuclei up to ^{30}Mg could be observed. Yields were measured for 42 isotopes, for further 17 isotopes upper limits could be deduced. The measured yields and energy distributions give a good overview on the ternary fission of ^{241}Pu(n,f). In future this survey could be completed by measuring some "missing" isotopes at the masses A=13, 23, etc. and improving the statistics for the heaviest isotopes. Together with recent measurements of other fission systems this enlarged data set of ternary fission yields will help to improve the current ternary fission models.

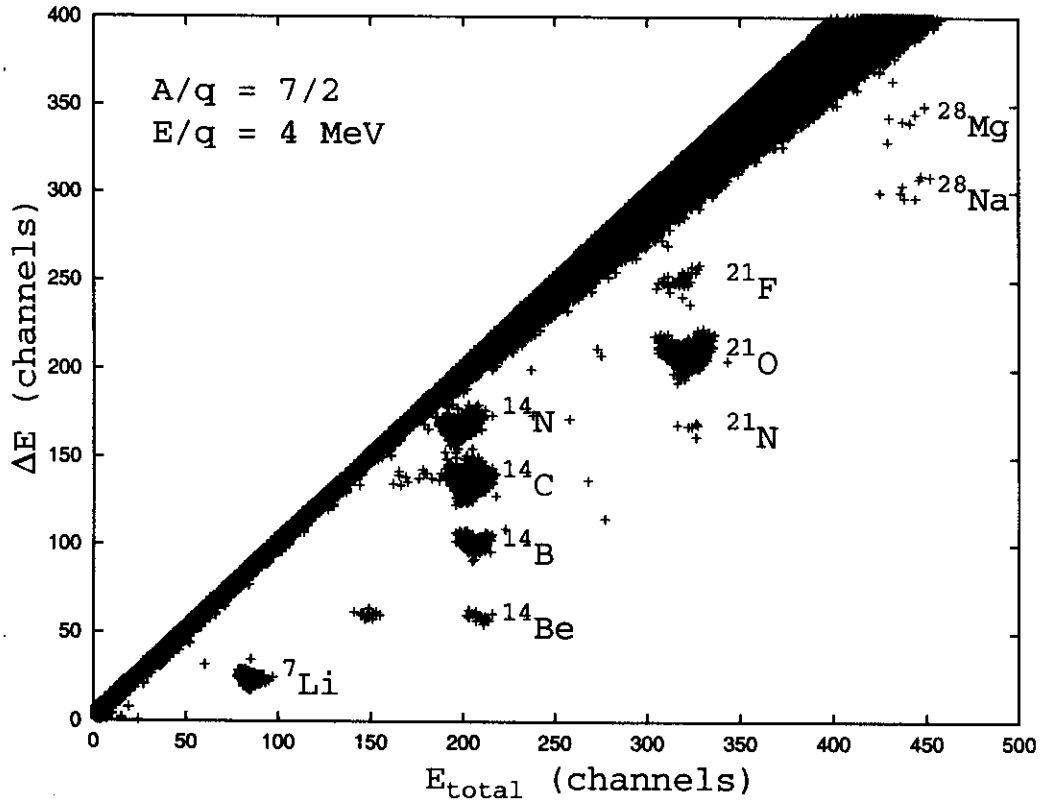

Fig. 10. Identification of ^{14}Be in a ΔE/E scatter plot taken during 19.5 h with the separator set to $A/q = 3.5$ and $E/q = 4$ MeV.

The fission system ^{242}Pu* is particularly interesting since a direct comparison between ternary yields from thermal neutron induced fission ^{241}Pu(n,f) and spontaneous fission of ^{242}Pu (see e.g. [55–57]) will become possible once the latter has been studied in more detail [13]. A comparison of the binary fission yields of ^{241}Pu(n_{th},f) and ^{242}Pu(sf) [58] showed significant differences due to a 6 MeV difference in excitation energy.

Acknowledgements

We are grateful for fruitful discussions with Michael Hesse and Marcus Wöstheinrich. Thanks for support by the Accelerator Laboratory of the TU and LMU München.

[13] Several ternary yields are known in two other cases of spontaneous fission: ^{248}Cm(sf) and ^{252}Cf(sf), but it is still difficult to find sufficient quantities of the corresponding target nuclides ^{247}Cm and ^{251}Cf for a detailed study of the neutron-induced fission yields.

References

[1] T. San-Tsiang et al., C. R. Acad. Sci. Paris 223 (1946) 986.

[2] T. San-Tsiang et al., Phys. Rev. 71 (1947) 382.

[3] G. Farwell, E. Segrè and C. Wiegand, Phys. Rev. 71 (1947) 327.

[4] *Ternary Fission*, C. Wagemans, chapter 12 in *The Nuclear Fission Process*, ed. by C. Wagemans, CRC Press, Boca Raton (1991) p. 545.

[5] *Particle-accompagnied fission*, M. Mutterer and J.P. Theobald, chapter 12 in *Nuclear Decay Modes*, ed. by D.N. Poenaru, IOP Publishing, Bristol, 1996, p. 487.

[6] A. Vorobyov et al., Phys. Lett. 30B (1969) 332.

[7] A. Vorobyov et al., Phys. Lett. 40B (1972) 102.

[8] W. Baum, PhD thesis, TH Darmstadt, 1992.

[9] W. Baum et al., 6th Int. Conf. on Nuclei far from Stability and 9th Int. Conf. on At. Masses and Fund. Const., Bernkastel-Kues, ed. by R. Neugart and A. Wöhr, Inst. Phys. Conf. Ser. No. 132, IOP Publishing, Bristol, 1992, p. 477.

[10] A. Vorobyov et al., Sov. J. Nucl. Phys. (1975) 248.

[11] F. Gönnenwein et al., 6th Int. Conf. on Nuclei far from Stability and 9th Int. Conf. on At. Masses and Fund. Const., Bernkastel-Kues, ed. by R. Neugart and A. Wöhr, Inst. Phys. Conf. Ser. No. 132, IOP Publishing, Bristol, 1992, p. 453.

[12] Berthold Börsig, PhD thesis, Universität Tübingen, 1993.

[13] R. Schäfer and T. Fliessbach, J. Phys. G21 (1995) 861.

[14] N. Cârjan, A. Săndulescu and V.V. Pashkevich, Phys. Rev. C11 (1975) 782.

[15] N. Cârjan, J. Phys. (Paris) 37 (1976) 1279.

[16] A. Săndulescu et al., J. Phys. G24 (1998) 181.

[17] G.V. Valskii, Sov. J. Nucl. Phys. 24 (1976) 140.

[18] V.A. Rubchenya and S.G. Yavshits, Z. Phys. A329 (1988) 217.

[19] G.A. Pik-Pichak, Phys. At. Nucl. 57 (1994) 906.

[20] M. Hesse and F. Gönnenwein, Workshop on nuclear fission and fission product spectroscopy, Seyssins, ed. by H. Faust and G. Fioni, ILL report 94FA05T (1994) p. 18.

[21] Boualem Bouzid, PhD thesis, Univ. des Sciences et de Technologie Houari Boumedienne, Alger, 1994.

[22] H. Faust and Z. Bao, Proc. Seminar on Fission "Pont d'Oye III", ed. by C. Wagemans, Euratom Geel, EUR16295 EN (1995) p. 220.

[23] M. Wöstheinrich et al., Acta Phys. Slov. 49 (1999) 987.

[24] M. Wöstheinrich et al., 2nd Int. Workshop on Nucl. Fission and Fission-Product Spectroscopy, Seyssins, ed. by G. Fioni et al., AIP Conf. Proc. 447, p. 330.

[25] Ulli Köster, PhD thesis, TU München, 1999.

[26] Michael Hesse, PhD thesis, Universität Tübingen, 1997.

[27] Marco Davi, PhD thesis, Universität Mainz, 1997.

[28] C. Wagemans et al., Phys. Rev. C33 (1986) 943.

[29] T. Friedrichs et al., 2nd Int. Workshop on Nucl. Fission and Fission-Product Spectroscopy, Seyssins, ed. by G. Fioni et al., AIP Conf. Proc. 447, p. 231.

[30] Thomas Friedrichs, PhD thesis, TU Braunschweig, 1997.

[31] E. Moll et al., Int. conf. on electromagn. isot. sep., Marburg, ed. by H. Wagner and W. Walcher, report BMBW-FB K70-28 (1970) p. 241.

[32] E. Moll et al., Nucl. Instr. Meth. 123 (1975) 615.

[33] S. Neumann and H. Ewald, Z. Phys. 169 (1962) 224.

[34] G. Fioni et al., Nucl. Instr. Meth. A322 (1993) 175.

[35] J.P. Bocquet, R. Brissot and H. Faust, Nucl. Instr. Meth. A267 (1988) 466.

[36] M. Hesse et al., Workshop on High Resolution Spectroscopy of Fission Fragments, Neutrons and γ rays, ed. by H. Maerten et al., report FZR-93-08 (1993) p. 31.

[37] H. Faust et al., ILL Report 81FA45S (1981).

[38] J.P. Biersack and L.G. Haggmark, Nucl. Instr. Meth. 174 (1980) 257.

[39] L.C. Northcliffe, Ann. Rev. Nucl. Sci. 13 (1963) 67.

[40] H.H. Heckman, E.I. Hubbard and W.G. Simon, Phys. Rev. 129 (1963) 1240.

[41] H.D. Betz et al., Phys. Lett. 22 (1966) 643.

[42] V.S. Nikolaev and I.S. Dmitriev, Phys. Lett. A28 (1968) 277.

[43] K.X. To and R. Drouin, Nucl. Instr. Meth. 160 (1979) 461.

[44] Y. Baudinet-Robinet, Nucl. Instr. Meth. 190 (1981) 197.

[45] Y. Baudinet-Robinet, Phys. Rev. A26 (1982) 62.

[46] K. Shima, T. Ishikara and T. Mikumo, Nucl. Instr. Meth. 200 (1982) 605.

[47] K. Shima et al., At. Data and Nucl. Data Tables 51 (1992) 173.

[48] Marcus Wöstheinrich, PhD thesis, Universität Tübingen, 1999.

[49] CRC Handbook of Chemistry and Physics, ed. by D.R. Lide and H.P.R. Frederikse, CRC Press, Boca Raton, 1997.

[50] F. Caïtucoli et al., Z. Phys. A298 (1980) 219.

[51] G. Audi et al., Nucl. Phys. A624 (1997) 1.

[52] S.K. Kataria, E. Nardi and S.G. Thompson, Proc. 3rd Symp. on Phys. and Chem. of Fission, Rochester, 1973, IAEA-SM-174/63, p. 389.

[53] N. Feather, Proc. R.S.E. (A) 71 (1974) 323.

[54] P. Schillebeeckx et al., Nucl. Phys. A580 (1994) 15.

[55] P. Schillebeeckx et al., Nucl. Phys. A545 (1992) 623.

[56] J.H. Hamilton et al., Prog. Part. Nucl. Phys. 35 (1995) 635.

[57] Y.X. Dardenne et al., Phys. Rev. C54 (1996) 206.

[58] E. Allaert, C. Wagemans and G. Wegener-Penning, Nucl. Phys. A380 (1982) 61.

Table 1
Measured yields and energy parameters for hydrogen to carbon isotopes. *"u.l."* is an upper limit for isotopes where no or too few events were found to determine a reliable yield.

Isotope	E_{mean} (MeV)	$\sigma(E_{mean})$ (MeV)	E_{FWHM} (MeV)	$\sigma(E_{FWHM})$ (MeV)	Yield	σ(Yield)	E_{bin} (MeV)
2H	8.4	*fix*	6.3	0.3	42	4	-
3H	8.4	*fix*	6.1	0.3	786	42	-
4He	15.9	*fix*	9.9	*fix*	10000	700	11.1
6He	11.3	0.2	10.3	0.4	260	30	1
8He	8.7	0.2	9.5	0.4	15	1	-
7Li	14.7	0.5	9.9	1.1	6.7	0.6	3.7
8Li	15.7	1.1	11.8	1.9	4.2	0.6	-
9Li	12.6	0.6	12.4	0.9	8.3	0.8	-
11Li	11	*fix*	11	*fix*	0.0045	0.0015	-
7Be	20	*fix*	13	*fix*	0.2	*u.l.*	1
9Be	17.9	0.6	12.9	1.4	4.4	0.5	10.5
10Be	18	0.7	16	2.5	46	6	12.4
11Be	17.5	0.7	12	2	5.9	1.7	6.7
12Be	14.3	0.8	13.4	1.8	2.8	0.3	4.8
14Be	13	*fix*	13	*fix*	0.0027	0.0010	-
10B	22	*fix*	18	*fix*	0.03	*u.l.*	9.4
11B	21	*fix*	17	*fix*	1.6	1.0	15.7
12B	20	*fix*	16	*fix*	1.0	0.4	13.4
14B	19	*fix*	15	*fix*	0.13	0.04	8
15B	17.7	0.6	12.9	1.1	0.046	0.010	5.8
17B	16	*fix*	13	*fix*	0.001	*u.l.*	-
14C	20.8	0.6	21.6	1.9	12.6	0.8	27.4
15C	18.6	1.3	23.1	2.7	4.3	0.4	22.5
16C	16.6	2.7	26	6	5.0	0.9	22.1
17C	18	*fix*	20	*fix*	0.64	0.15	16.7
18C	17.7	1.7	15.2	1.9	0.28	0.05	16
19C	17	*fix*	17	*fix*	0.0025	0.0014	10.1
20C	16	*fix*	16	*fix*	0.0036	0.0028	8.4

Table 2
Measured yields and energy parameters for nitrogen to silicon isotopes. *"u.l."* is an upper limit for isotopes where no or too few events were found to determine a reliable yield.

Isotope	E_{mean} (MeV)	$\sigma(E_{mean})$ (MeV)	E_{FWHM} (MeV)	$\sigma(E_{FWHM})$ (MeV)	Yield	σ(Yield)	E_{bin} (MeV)
15N	22	*fix*	18	3	0.044	*u.l.*	29.3
16N	21	*fix*	20	*fix*	0.079	0.032	26.2
17N	20	*fix*	20	*fix*	0.34	0.10	27.3
18N	19	*fix*	18.6	2.0	0.16	0.04	24.3
19N	18	*fix*	18	*fix*	0.26	0.08	24.7
20N	17.5	*fix*	17.5	*fix*	0.0029	0.0016	21
21N	17	*fix*	17	*fix*	0.0025	0.0014	20.6
15O	24	*fix*	20	*fix*	0.12	*u.l.*	23.6
19O	23	*fix*	20	*fix*	0.26	0.12	34.5
20O	22.1	0.9	18.5	2.1	1.10	0.12	37.5
21O	21	*fix*	16.9	3.5	0.23	0.06	35.1
22O	20	*fix*	16	*fix*	0.12	0.04	37.4
24O	18	*fix*	18	*fix*	0.08	*u.l.*	33.2
19F	26	*fix*	22	*fix*	0.020	0.016	35.9
20F	25	*fix*	23	*fix*	0.002	*u.l.*	36.9
21F	23	*fix*	19.2	7.5	0.021	0.006	40.3
22F	23	*fix*	23	*fix*	0.30	0.21	40
24F	21	*fix*	22.3	3.3	0.030	0.016	40.9
24Ne	25	*fix*	20	2.8	0.040	0.012	52.8
27Ne	24	*fix*	22	*fix*	0.008	*u.l.*	48.4
24Na	28	*fix*	24	*fix*	0.001	*u.l.*	
27Na	26	*fix*	24	*fix*	0.005	*u.l.*	57.7
28Na	26	*fix*	24	*fix*	0.006	0.004	55.9
30Na	24	*fix*	24	*fix*	0.0008	*u.l.*	53.1
27Mg	30	*fix*	26	*fix*	0.0012	*u.l.*	
28Mg	30	*fix*	26	*fix*	0.018	*u.l.*	67.4
30Mg	28	*fix*	26	*fix*	0.009	0.006	67.9
30Al	32	*fix*	28	*fix*	0.002	*u.l.*	
34Si	36	*fix*	30	*fix*	0.001	*u.l.*	58.3
35Si	35	*fix*	30	*fix*	0.003	*u.l.*	78.4
36Si	33	*fix*	30	*fix*	0.004	*u.l.*	80.4